Robotica: (2021) volume 39, pp. 1634–1641. © The Author(s), 2021. Published by Cambridge University Press.
doi:10.1017/S026357472000140X

Design and Research of a Walking Robot with Two Parallel Mechanisms

Huanhuan Ren, Lizhong Zhang* and Chengzhi Su

College of Mechanical and Electric Engineering, Changchun University of Science and Technology, Changchun 130022, China

(Accepted December 14, 2020. First published online: February 15, 2021)

SUMMARY
In this paper, a new type of biped mobile robot is designed. Each leg of the robot is a 6 degree-of-freedom (DOF) parallel mechanism, and each leg has three relatively fixed landing points. The leg's structure gives the robot better performance on large carrying capacity, strong environmental adaptability and fast moving speed simultaneously. At the same time, it helps the robot move more steadily and change direction more simply. Based on the structural features of the leg, the inverse kinematics model of the biped robot is established and a unified formula is obtained. According to an analysis of robot's workspace, gait planning is completed and simulated. Finally, the special case that the robot can keep the upper body horizontal while walking on a slopy surface is validated.

KEYWORDS: Biped robot; 6 DOF parallel mechanism; Working space; Path planning.

1. Introduction

Mobile robots have become a hotspot in the field of robotics because of their flexible mobility and high intelligence, and walking mobile robots have better adaptability than wheeled or tracked mobile robots on uneven terrains such as soft ground, stairs and obstacles. In the field of mobile robots, it is a basic problem to make robots walk flexibly and avoid obstacles in uncertain environments; some of them also are required to have the ability to bear external loads other than their own gravity. Researchers have made many remarkable achievements in structural design, gait analysis and stability control of mobile robots.[1–5] At present, more and more mobile robots with advanced sensors are stepping out of the laboratory to assist human beings to complete various tasks.[6–8] These robots can be used to explore the moon, mars and oceans, in urban search and rescue, including searching of survivors in collapsed buildings and of missing persons in disaster areas.[9]

Mobile robots that can carry loads have wider applications. Generally, the driving system determines the loading capacity of the robot. An hydraulic system has the advantages of large driving force and small size; so robots with these actuators can carry more loads, such as the Big Dog,[10] but there may be problems of high noise and difficulty of maintenance. An electrical motor-actuated robot can achieve excellent dynamic performance and is energy-efficient while moving without noise. Such robots are more stable and easy to be controlled, such as NOROS-II.[11] However, the loading capacity is directly determined by the power of the motor. Another main factor that affects loading capacity is the structure of robot legs. Parallel mechanism is used as the mechanical leg of many mobile robots with strong loading capacity.[12–15]

This paper presents the design of an electrical motor-actuated bipedal robot. Each leg of the robot is a 6 DOF parallel mechanism, which has the characteristics of strong loading ability and high stability. Even when traveling on slopes, stairs or rough terrains, the upper body of the robot can be kept in a horizontal state, which other mobile robots cannot achieve. First, the general mechanism of a robot and the structure of its legs are introduced. Then, the kinematics of the robot's single leg and the workspace of the single leg are introduced. Finally, path planning of the robot is analyzed, which keeps the upper body horizontal on a sloping or stepped terrain.

* Corresponding author. E-mail: custmechanic@163.com

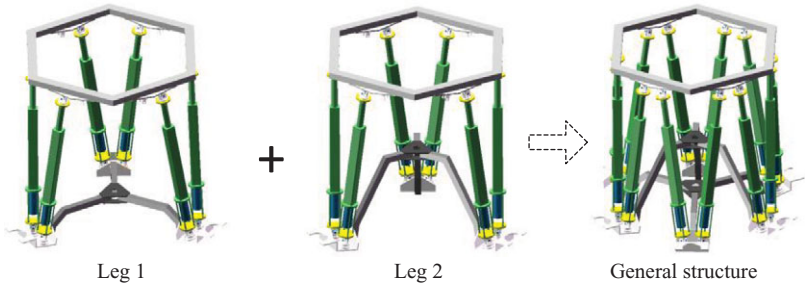

Fig. 1. General structure of the robot.

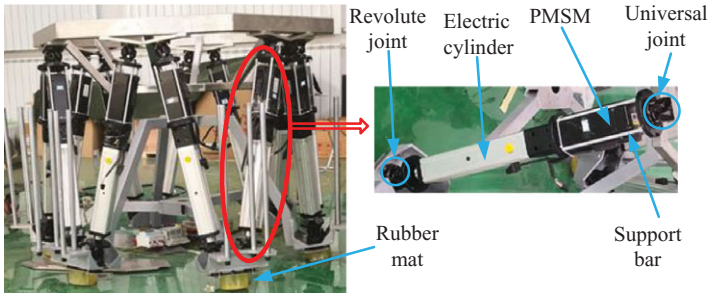

Fig. 2. Limb structure.

2. Structural Design

2.1. General structure and leg structure

As shown in Fig. 1, the robot consists of two groups of parallel mechanisms (two legs). In principle, the robot has high structural stiffness, since it is supported by several limbs at the same time. There are three landing points for each leg of this robot, which is different from these robots with only one landing point for each leg. The relative position of three landing points is fixed and the distance between each two landing points is relatively long, which can cause the center of gravity of the robot to remain in the area composed of the three points. This can improve the stability of the robot, especially when moving on a flat ground. There is also a rubber mat (shown in Fig. 2) at the bottom of each landing point to reduce landing impact and enhance friction to avoid sliding.

Different from most mobile robots that use serial legs, this robot uses parallel mechanism as its leg. Each parallel mechanism can be seen as a closed-loop kinematic chain mechanism whose moving platform is linked to the base by several independent kinematic chains. In this paper, the parallel mechanism consists of an upper platform connected to a lower platform by six identical limbs. These limbs consist of an actuated prismatic joint (P) connected to the upper platforms through a passive universal joint (U) and connected to the lower platform through a passive universal joint with a revolute joint (R) as shown in Fig. 2. The links feel only traction or compression, not bending, which increases their position accuracy and allows a lighter construction.[16] Each parallel mechanism can be represented by 6UPUR.

2.2. Mathematical model of a single leg

A universal joint provides 2 DOF; a prismatic joint and a revolute joint provide 1 DOF. The freedom of 6UPUR can be calculated by Chebyshev–Grübler–Kutzbach criterion:[17]

$$M = 6(n - g - 1) + \sum_{i=1}^{m} f_i \tag{1}$$

in which M =DOF of the mechanism, n = number of links in the mechanism including the base, g = number of joints of the mechanism, m = number of links, fi =degrees of relative motion

https://doi.org/10.1017/S026357472000140X Published online by Cambridge University Press

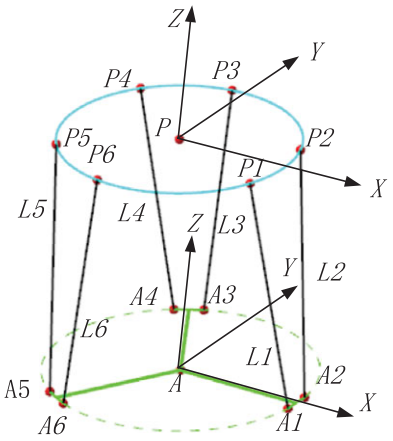

Fig. 3. Simplified structure and mathematical model of a single leg.

permitted by joint i. For the parallel mechanism designed in this paper, $n = 20$, $g = 24$, $\sum f_i = 36$, so $M = 6$. This means that each leg of the robot has 6 DOF and can generate a complete spatial movement with 3 DOF for position and 3 DOF for orientation. This is the reason that the robot can maintain the level of the platform while advancing on an uneven terrain.

In order to describe and control the motion of the robot, it is necessary to describe the relative motion between the upper platform and the lower platform of a single leg. Take leg 1 as an example; the simplified structure and mathematical model of leg 1 is illustrated in Fig. 3. The upper platform is marked as P, while the lower platform of leg 1 is marked as A and that of leg 2 can be marked as B. P and A are coupled via six limbs, each attached to points A_i and P_i ($i = 1, 2 \ldots 6$). Attach frame $\{P\}$ to P, frame $\{A\}$ to A.

First of all, assume that the lower platform is movable and the upper platform is fixed. The pose of the lower platform $\{A\}$ relative to the upper platform $\{P\}$ can be defined by a position vector $P[P_X, P_Y, P_Z]$ in addition to a 3×3 rotation matrix T.

$$T = \begin{bmatrix} r_{11} & r_{12} & r_{13} \\ r_{21} & r_{22} & r_{23} \\ r_{31} & r_{32} & r_{33} \end{bmatrix} \tag{2}$$

Euler angles are usually used to describe the orientation between $\{P\}$ and $\{A\}$. *Z-Y-X* Euler angles means that one frame first rotates α around Z-axis, then rotates β around Y-axis, and finally rotates γ around X-axis. Each step of rotation is based on the previous rotation. In this case, the orientation of A with respect to P can be expressed by Eq. (3):

$$T = RZ(\alpha)RY(\beta)RX(\gamma) = \begin{bmatrix} c\alpha c\beta & c\alpha s\beta s\gamma - s\alpha c\gamma & c\alpha s\beta c\gamma + s\alpha s\gamma \\ s\alpha c\beta & s\alpha s\beta s\gamma + c\alpha c\gamma & s\alpha s\beta c\gamma - c\alpha s\gamma \\ -s\beta & c\beta s\gamma & c\beta c\gamma \end{bmatrix} \tag{3}$$

where $R_Z(\alpha)$, $R_Y(\beta)$, $R_X(\gamma)$ are the basic rotation matrices, $c\alpha = \cos(\alpha)$, $s\alpha = \sin(\alpha)$. The pose of $\{A\}$ relative to $\{P\}$ can be marked as Eq. (4).

$$F = (X, Y, Z, \alpha, \beta, \gamma) \tag{4}$$

${}^A\boldsymbol{R}$ represents the vector in $\{A\}$; so ${}^A\boldsymbol{R}$ can be expressed in $\{P\}$ as Eq. (5).

$${}^P R = T\,{}^A R + P \tag{5}$$

3. Kinematics and workspace analysis of a single leg

3.1. Inverse kinematics

An inverse kinematics solution plays an important role in robot control and workspace analysis.[18,19] In an inverse kinematics analysis, the pose of a moving platform is known to calculate the length of

https://doi.org/10.1017/S026357472000140X Published online by Cambridge University Press

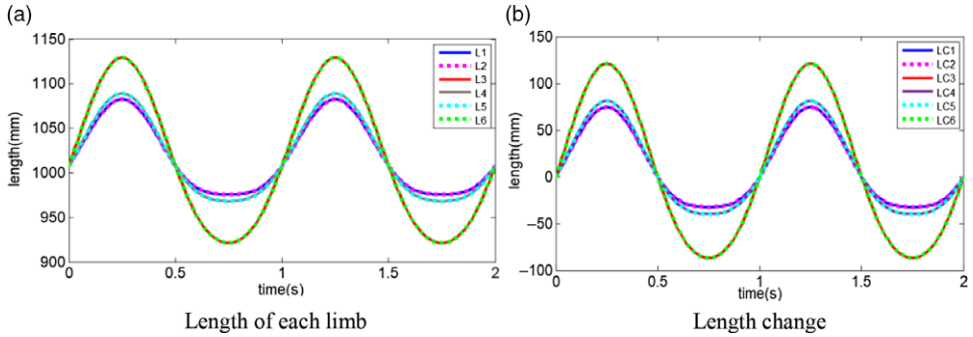

Fig. 4. Curve of length with time.

every limb. Take leg 1 as an example; according to the structure, there is a geometric relationship shown in Fig. 3; the closure of each kinematic loop can be expressed in vector form as Eq. (6):

$$PP_i + P_i A_i = PA + AA_i \tag{6}$$

in which PP_i and AA_i can be obtained easily from the geometry of the attachment points in the two platforms. Through Eq. (5), the position of A_i in $\{P\}$ can be obtained, then the length of limb i can be calculated as Eq. (7).

$$L_i = [L_{iX}\ L_{iY}\ L_{iZ}] = [P_X\ P_Y\ P_Z]^T + T[A_{iX}\ A_{iY}\ A_{iZ}]^T - [P_{iX}\ P_{iY}\ P_{iZ}]^T \tag{7}$$

According to Eq. (7), the length of every limb can be expressed as:

$$li = \sqrt{L_{iX}{}^2 + L_{iY}{}^2 + L_{iZ}{}^2} \tag{8}$$

When the lower platform is fixed and the upper platform is relatively mobile, a similar analysis can be used. The dynamic walking of this robot is determined by the step size and leg height. Assuming that A moves relative to P, the length and length change (LC) of each limb can be obtained by Eq. (4) and Eq. (8). Length change can be used as the input signal of the servo system to control the output of a permanent magnet synchronous motor (PMSM).

$$\begin{cases} X = 200^* \sin(2\pi t) \\ Y = 0 \\ Z = 75^* \sin(2\pi t) \end{cases} \tag{9}$$

where 200 mm is the step size that A moves on the X-axis and 75 mm is the lift of leg height on Z-axis. The length of each limb and length change are shown in Fig. 4. Length change is obtained by subtracting the initial length (100 mm) from the length, and in the initial state, the length of each limb is the same.

3.2. Workspace analysis

For mobile robots, it is very important that the legs have a sufficient workspace for walking and running.[20,21] The reachable workspace and dexterous workspace of the leg can be obtained by inverse kinematics and the limit of mechanism.[22] Reachable workspace refers to all the positions that the leg can arrive, while dexterous workspace means a region where the leg can reach with all orientations. Reachable workspace and its boundaries are crucial because it determines the maximum range that the leg can arrive, thus affecting the speed and pace of the robot. Dexterous workspace can be used for the analysis of pose adjustment when the robot walks on an uneven terrain. Take leg 1 as an example; the reachable workspace can be estimated in the following steps:

Step 1. A group of planes parallel to the XY plane and spaced with ΔZ are used to divide all the possible regions that the lower platform can reach.

https://doi.org/10.1017/S026357472000140X Published online by Cambridge University Press

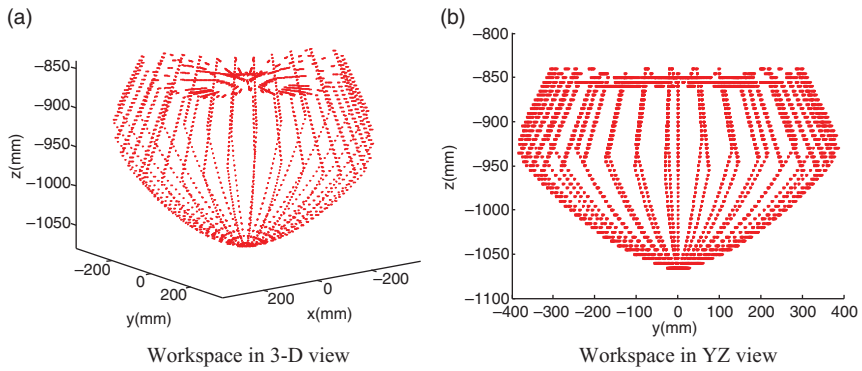

Fig. 5. Workspace of leg 1.

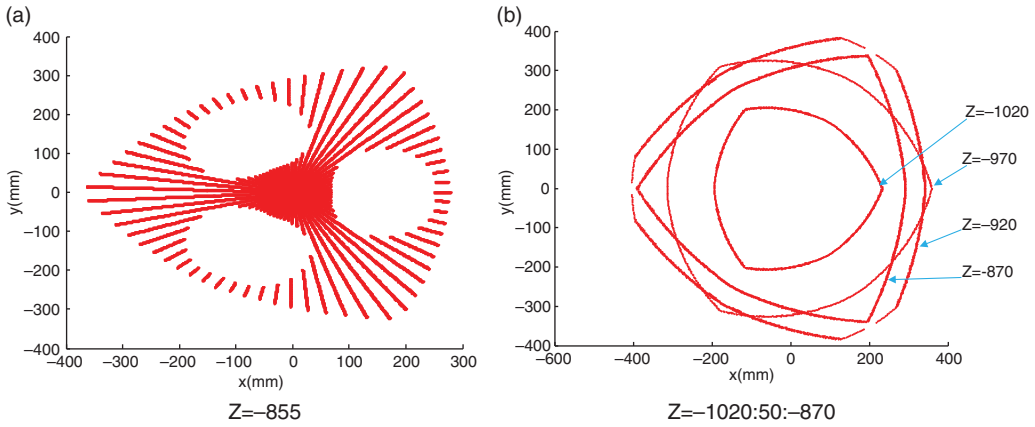

Fig. 6. *XY* section of workspace at different heights.

Step 2. Starting from the height value *Z*, the workspace of the lower platform satisfying Eq. (10) on the corresponding plane (the height is *Z*) is obtained using the spatial search method.

Step 3. Repeat Step 2 to find the workspace of $Z + i^{*}\Delta Z$ ($i = 1, 2 \ldots$) planes.

The workspace is determined by the reachable extent of limbs and joints, then by the collisions. Ignoring collisions, only considering the length of limbs and the angle of universal joints, the restrictions are shown in Eq. (10):

$$\begin{cases} L_{\min} < l_i < L_{\max} \\ |\theta_{Pi}| < \theta_P, \ |\theta_{Ai}| < \theta_A \end{cases} \tag{10}$$

in which L_{min} is the minimum length of the limb, L_{max} is the maximum length; θ_P, θ_A are the maximum angles at which the universal joint can rotate relative to the platform. The workspace of the lower platform of leg 1 relative to the upper platform is obtained as shown in Fig. 5.

The workspace can be used as a reference when the robot moves forward and raises its legs. Every step of the robot's displacement should be in the workspace. And the legs should move in the dexterous workspace as far as possible in the gait planning of the robot. At different heights, the boundaries of the workspace are shown in Fig. 6(b). According to Fig. 6(a), if the lifting height of the leg is too high, the leg may not reach the command position normally.

Using this similar approach, we can analyze the workspace of the upper platform relative to the lower platform when the lower platform is fixed and the upper platform is movable. And the workspace of the upper platform is also available when both legs are on the ground, which is very crucial for the pose adjustment of the upper platform when there is an external load, as shown in Fig. 7.

https://doi.org/10.1017/S026357472000140X Published online by Cambridge University Press

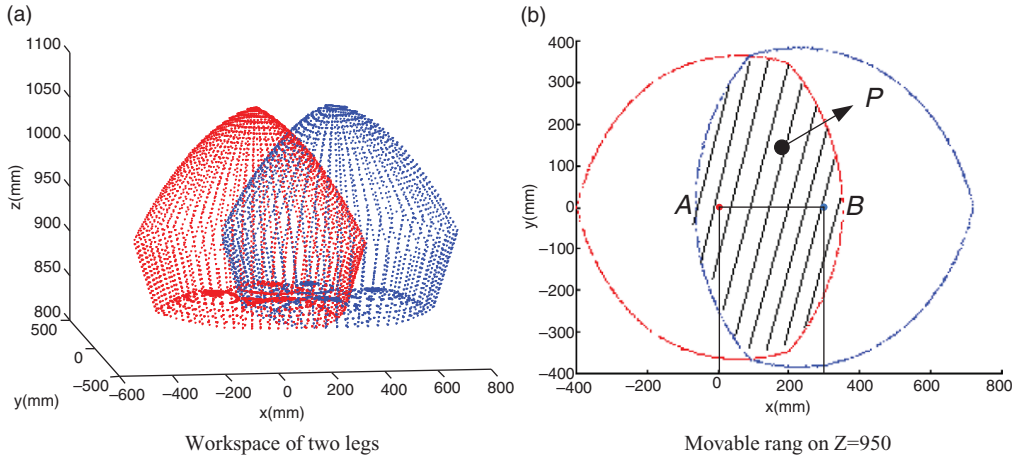

Fig. 7. Workspace of upper platform.

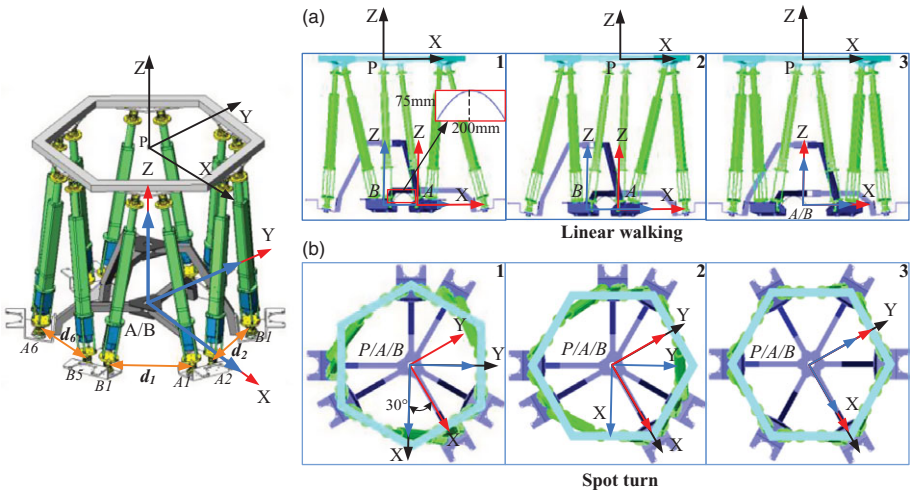

Fig. 8. Gait planning of the robot.

4. Gait planning and simulation

It is the most basic requirement for mobile robots to walk and turn steadily on a flat terrain. Walking on an irregular terrain is a common task of advanced robots, which requires many degrees of freedom and good control performance. Each leg of the robot is a 6 DOF parallel mechanism and has three landing points; so it is very easy to walk and turn on a flat terrain and has great loading capacity and stability because the center of mass will always stay within the region of three points. Next, gait planning will be carried out for the robot to move forward and spot-turn on a flat terrain, and it will be verified that the robot can keep the upper platform horizontal when walking on a slopy surface with high stability.

As shown in Fig. 8, it takes only three steps for the robot to complete linear walking and spot-turn. Gait planning of this robot is to determine the relative poses of A, B and P in the course of motion. To avoid collision between the two legs, the distance between the universal joints can be limited, marked as $d1$, $d2 \ldots d6$ in Fig. 8. First, let the robot rotate 30 degrees around Z-axis in situ (0–6 seconds) and then move 200 mm in the X direction (6–12 seconds). The length of each limb (L_i stands for the limbs of leg 1, T_i stands for the limbs of leg 2) and the distance of $d1$, $d2 \ldots d6$ are shown in Fig. 9. According to the change range of L_i, T_i, d_i and the analysis of workspace, the feasibility of gait planning can be verified offline.

For moving on a slopy surface, this robot can keep its upper platform horizontal rather than just let itself pass (as shown in Fig. 10(a)), which is very useful in many cases. Of course, the inclination of a slopy surface that the robot can pass depends on the workspace, and the robot should take smaller

https://doi.org/10.1017/S026357472000140X Published online by Cambridge University Press

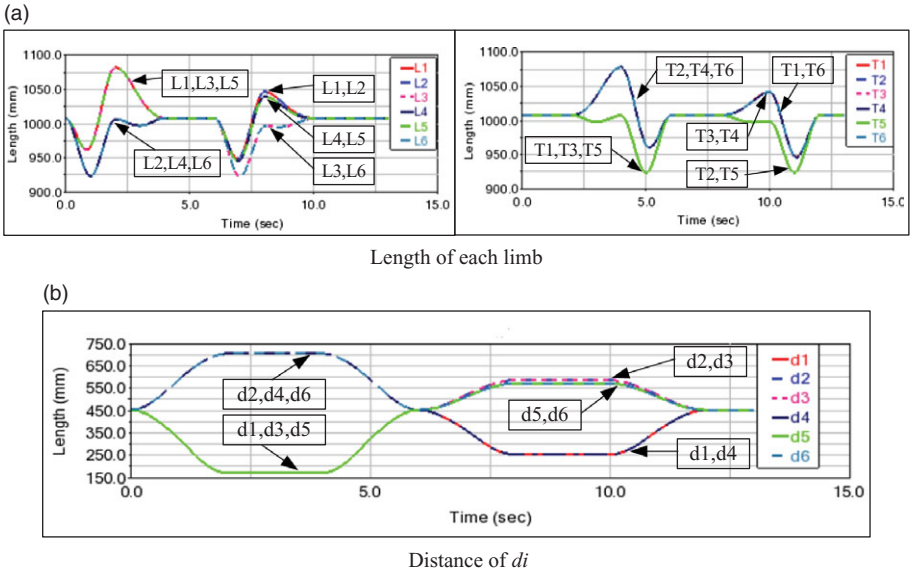

Length of each limb

Distance of *di*

Fig. 9. Change of L_i, T_i, d_i.

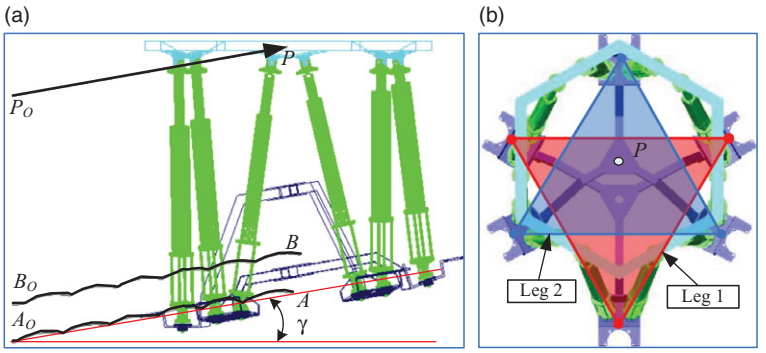

Go forward on slope surface

Support phase of Leg 1 and Leg 2

Fig. 10. Going forward on a slopy surface and stability region.

steps and speed when walking on a slopy surface or stairs. A wider workspace of the robot can be achieved by increasing the length of the limbs or adding other driving mechanisms. As can be seen in Fig. 9(b), the stability region of each leg is large enough to keep P always in it, which guarantees the stability of the robot.

5. Conclusion

In this paper, a new type of mobile robot is designed. Each leg of the robot is a 6 DOF parallel mechanism, which can improve the loading capacity of the robot. First, the configuration of the limbs and the kinematics model of the robot are analyzed. Then the workspace is obtained, and then gait planning on a flat terrain and movement on a slopy surface are completed. The purpose of this paper is to provide a new type of mobile robot and promote the application of parallel mechanism in mobile robots.

References

1. M. Khadiv, S. A. A. Moosavian, A. Yousefi-Koma, M. Sadedel and S. Mansouri, "Optimal gait planning for humanoids with 3D structure walking on slippery surfaces," *Robotica* **35**(3), 569–587 (2017).
2. D. Kuehn, M. Schilling, T. Stark, M. Zenzes and F. Kirchner, "System design and testing of the hominid robot Charlie," *J Field Robot*. **34**(4), 666–703 (2017).
3. Y. Pan and F. Gao, "Position model computational complexity of walking robot with different parallel leg mechanism topology patterns," *Mech Mach Theory* **107**, 324–337 (2017).

https://doi.org/10.1017/S026357472000140X Published online by Cambridge University Press

4. H. Amirhosseini and F. Najafi, "Design, prototyping and performance evaluation of a bio-inspired walking microrobot," *Iran J Sci Technol Trans Mech Eng*. **44**(9), 1–13 (2019).
5. D. Xi and F. Gao, "Type synthesis of walking robot legs," *Chin J Mech Eng*. **31**(1), 15 (2018).
6. J. M. Badger, P. Strawser, L. Farrell, S. M. Goza, C. Claunch, R. Chancey and R. Potapinski, "Robonaut 2 and Watson: Cognitive dexterity for future exploration," 2018 IEEE Aerospace Conference, 1–8 (2018).
7. X. Xiong and A. D. Ames, "Bipedal hopping: Reduced-order model embedding via optimization-based control," 2018 IEEE/RSJ International Conference on Intelligent Robots and Systems (IROS) Madrid, Spain, October 1–5 (2018).
8. D. SanzMerodio, E. Garcia and P. GonzalezdeSantos, "Analyzing energy-efficient configurations in hexapod robots for demining applications," *Ind Robot: Int J.* **39**(4), 357–364 (2012).
9. D. Belter and P. Skrzypczynski, "Posture optimization strategy for a statically stable robot traversing rough terrain," Intelligent Robots and Systems (IROS), IEEE/RSJ International Conference on IEEE (2012).
10. M. Raibert, "Dynamic legged robots for rough terrain," IEEE-RAS International Conference on Humanoid Robots IEEE (2010).
11. S. Peng, X. Ding, F. Yang and K. Xu, "Motion planning and implementation for the self-recovery of an overturned multi-legged robot," *Robotica* **35**(5), 1107–1120 (2017).
12. Y. Rong, Z. L. Jin and M. K. Qu, "Study on Mechanics Structural Synthesis of Six-Legged Walking Robot with Parallel Leg Mechanisms," *Adv Mater Res*. **496**, 247–250 (2012).
13. K. Hashimoto, Y. Sugahara, C. Tanaka, A. Ohta, K. Hattori, T. Sawato, A. Hayashi, H. O. Lim and A. Takanishi, "Unknown disturbance compensation control for a biped walking vehicle," 2007 IEEE/RSJ International Conference on Intelligent Robots and Systems, October 29–November 2, 2007, Sheraton Hotel and Marina, San Diego, California, USA IEEE (2007).
14. G. Feng, "A new six-parallel-legged walking robot for drilling holes on the fuselage," *Proc Inst Mech Eng, Part C: J Mech Eng Sci*. **228**(4), 753–764 (2014).
15. Y. Tian and F. Gao, "Efficient motion generation for a six-legged robot walking on irregular terrain via integrated foothold selection and optimization-based whole-body planning," *Robotica* **36**(3), 333–352 (2018).
16. H. D. Taghirad, *Parallel Robots: Mechanics and Control* (CRC Press, Boca Raton, FL, 2013).
17. P-G. Simo-Serra, "Kinematic synthesis using tree topologies," *Mech Mach Theory* **72**, 94–113 (2014).
18. M. Ghayour and A. Zareei, "Inverse kinematic analysis of a hexapod spider-like mobile robot," *Adv Mater Res*. **403–408**, 5061–5067 (2018).
19. C. Lopez-Franco, J. Hernandez-Barragan, A. Y. Alanis and N. Arana-Daniel, "A soft computing approach for inverse kinematics of robot manipulators," *Eng Appl Artif Intell*. **74**, 104–120 (2018).
20. D. Verde, S. D. Stan, M. Manic, R. Balan and V. Matie, "Kinematics analysis, workspace, design and control of 3-RPS and TRIGLIDE medical parallel robots," Conference on Human System Interactions IEEE Press (2009).
21. S. Zhang, J. Gao, X. Duan, H. Li, Z. Yu, X. Chen, J. Li, H. Liu, X. Li, Y. Liu and Z. Xu, "May. Trot pattern generation for quadruped robot based on the ZMP stability margin," 2013 ICME International Conference on Complex Medical Engineering. IEEE (2013).
22. D. J. Kim, W. K. Chung and Y. Youm, "Geometrical approach for the workspace of 6-DOF parallel nmanipulators," IEEE International Conference on Robotics & Automation IEEE Xplore (1997).

https://doi.org/10.1017/S026357472000140X Published online by Cambridge University Press